GA–A22693

COMPARISONS OF PHYSICAL AND CHEMICAL SPUTTERING IN HIGH DENSITY DIVERTOR PLASMAS WITH THE MONTE CARLO IMPURITY (MCI) TRANSPORT MODEL

by
T.E. EVANS, D.F. FINKENTHAL, Y.S. LOH, M.E. FENSTERMACHER,
G.D. PORTER, and W.P. WEST

NOVEMBER 1997

DISCLAIMER

GA–A22693

COMPARISONS OF PHYSICAL AND CHEMICAL SPUTTERING IN HIGH DENSITY DIVERTOR PLASMAS WITH THE MONTE CARLO IMPURITY (MCI) TRANSPORT MODEL

by
T.E. EVANS, D.F. FINKENTHAL,† Y.S. LOH,‡ M.E. FENSTERMACHER,◊
G.D. PORTER,◊ and W.P. WEST

†Palomar College
‡Harvard University
◊Lawrence Livermore National laboratory

This is a preprint of a paper to be presented at the Sixth International Workshop on Plasma Edge Theory in Fusion Devices, September 15–17, 1997, Oxford, United Kingdom and to be published in the *Proceedings*.

Work supported by
the U.S. Department of Energy
under Contract No. DE-AC03-89ER51114

GA PROJECT 3466
NOVEMBER 1997

Comparisons of physical and chemical sputtering in high density divertor plasmas with the Monte Carlo Impurity (MCI) transport model

T. E. Evans, D.F. Finkenthal,[◊] Y.S. Loh,[§] M.E. Fenstermacher,[‡] G.D. Porter,[‡] and W.P. West

General Atomics, San Diego, California, USA
[◊]Palomar College, San Marcos, California, USA
[§]Harvard University, Cambridge, Massachusetts, USA
[‡]Lawrence Livermore National Laboratory, Livermore, California, USA

Abstract

The MCI transport model was used to compare chemical and physical sputtering for a DIII–D divertor plasma near detachment. With physical sputtering alone the integrated carbon influx was 8.4×10^{19} neutrals/s while physical plus chemical sputtering produced an integrated carbon influx of 1.7×10^{21} neutrals/s. The average carbon concentration in the computational volume increased from 0.012% with only physical sputtering to 0.182% with both chemical and physical sputtering. This increase in the carbon inventory produced more radiated power which is in better agreement with experimental measurements.

1. Introduction

Comprehensive numerical models of the divertor and scrape-off layer plasma are essential for developing a better understanding of the complex processes found in the edge of diverted tokamaks. Two basic types of codes are used. One is based on a fluid description of the plasma. An example of this approach is the UEDGE [1] code. Most contemporary fluid codes run in either a single or multi-species mode to model a finite set of impurity species along with the usual deuterium background plasma. Fluid codes typically employ a 2D simulation grid and are restricted to solutions in which the ion mean free path is small compared to the plasma gradient scale lengths or the geometric scale of the simulation domain. These restrictions become prohibitive near material surfaces and in situations where the plasma parameters change rapidly over short spatial scales such as regions of detachment, near MARFEs, or in high recombination zones. On the other hand, impurity neutrals sputtered from material surfaces or injected as gas into the plasma edge move freely in a 3-dimensional space until dissociated and ionized. In addition, impurity ions are not born with thermally equilibrated Maxwellian distributions. These cold impurity ions require a finite time to thermalize with the background plasma *i.e.,* a heating up time. Thus, a 3D kinetic treatment is more appropriate for impurity neutrals and ions. Monte Carlo codes such as DIVIMP [2] in Europe, IMPMC [3] in Japan and the DIII–D Monte Carlo Impurity (MCI) transport model [4] in the U.S. have been developed specifically for

detailed impurity transport simulations in diverted tokamaks. A general review of edge plasma fluid and Monte Carlo codes can be found in a paper by Stangeby [5].

The MCI model consists of a set of task oriented modules which pass messages and data to each other through a single self-describing scientific (NetCDF) data file. This structure has proven to be very efficient for rapidly implementing new wall geometries, computational grids, atomic data, background plasma models and impurity transport physics and surface physics models. The impurity transport models used in MCI are identical to those originally implemented in DIVIMP. Parallel transport is assumed to be classical. Frictional forces due to background plasma flows are included along with forces generated by background ion and electron thermal gradients. MCI uses an averaged single particle approach which reduces, with appropriately defined ensemble averages, to a parallel impurity ion fluid momentum equation of the form:

$$m_z \frac{\partial v_{\|z}}{\partial t} = eEZ_z + 0.71 Z_z^2 \frac{\partial T_e}{\partial s} + \beta_z \frac{\partial T_i}{\partial s} + \frac{m_z}{\tau_{sl}} \left(v_{\|i} - v_{\|z} \right) \quad (1)$$

Here s is the spatial variable along the magnetic field, m_z is the impurity ion mass, $v_{\|z}$ is the parallel impurity ion velocity, β_z is a m_z dependent coefficient [6], and τ_{sl} is the impurity ion slowing down (or heating up) time on background plasma ions with parallel velocity $v_{\|i}$. Perpendicular transport is assumed to be anomalous and is modeled using a Monte Carlo type diffusive process. Diffusion along the field lines is implicitly accounted for in the Monte Carlo transport process due to random collisions with the background ions.

MCI's transport models have been carefully benchmarked against multi-species UEDGE carbon simulations. The two codes are in relatively good agreement when MCI is run on a standard UEDGE (non-orthogonal) grid with all the boundary conditions and neutral carbon launch parameters set to duplicate those used in UEDGE [7]. MCI calculated a total carbon inventory of 1.36×10^{17} particles while the UEDGE calculation resulted in 6.23×10^{17} particles. The carbon source rate in both codes was 2.41×10^{20} particles/s (38.6 A) with a constant 10^{-3} sputtering yield. Preliminary comparisons between MCI and DIVIMP, using the same conditions as those in the UEDGE comparisons, are more favorable than those between MCI and UEDGE. DIVIMP predicted a total carbon content of 1.39×10^{17} particles in this case [8]. Work is continuing to understand the differences between the Monte Carlo codes and the fluid code.

MCI simulations of intrinsic CIII density distributions were also compared [4,7,9] to experimentally measured 2D images of the CIII emissions in DIII–D using a tangential TV [10]. Reasonably good qualitative agreement is found between MCI simulations of the CIII emissions and the tangential TV data with physical sputtering only, although the total carbon inventory calculated in MCI is lower than expected based on experimental estimates [7]. This paper provides a brief comparison between MCI simulations with only physical sputtering and those with both physical and chemical sputtering.

2. MCI Carbon Source Modeling and Benchmarking

All of the currently available carbon sputtering models were developed and benchmarked with data from low flux ion beams impinging on clean, smooth, graphite targets. In order to be of use for high density radiative divertor simulations, these sputtering models must be scaled up by several orders of magnitude in ion flux and down by an order of magnitude in ion energy. In addition, uncertainties resulting from surface coating effects, reflection and sticking processes, and surface roughness effects have yet to be resolved. There are also unresolved questions concerning the effects of angular dependencies in the incident ion flux and the effects of non-Maxwellian particles. Progress on understanding the importance of some of these issues can be made by using physics based models to simulate chemical and physical sputtering and comparing the simulated data with experimental measurements.

MCI has options for using one of several empirical [11,12] or physics based [13,14] physical sputtering models. In addition, each of these physical sputtering models may be coupled to the most recent version of the Roth and García-Rosales (RG-R) chemical sputtering model [15]. The RG-R model may also be run in stand alone mode with its own internal physical sputtering model. These options provide greater flexibility for simulating the generation of intrinsic carbon impurities by the background plasma ions and self-sputtering processes. Background plasma parameters, obtained from a fluid code such as UEDGE, are used to calculate the incident hydrogenic ion flux and its energy. In MCI, the incident background ion flux may be modeled either as a sampled, single temperature, Maxwellian or as an averaged single temperature Maxwellian. Sputtered carbon neutrals are given a Thompson energy distribution [16] and a cosine angular distribution in the poloidal and toroidal directions. CD_4 molecules generated by the RG-R model need to be followed through a complex set of processes including molecular dissociation, dissociative ionization, and charge exchange interactions with background plasma ions before becoming carbon neutrals or singly ionize carbon particles.

Given the complexities and uncertainties involved in the sputtering, background plasma, and molecular transport/breakup models it is clearly advantageous to have accurate methods of benchmarking the simulations. Fortunately, DIII-D has a wide array of diagnostics which may be used in conjunction with MCI. Diagnostics of particular significance for benchmarking sputtering models are: the DiMES probe [17] which is used to characterize carbon erosion and redeposition, an array of absolutely calibrated, line integrated, spectroscopic instruments used to study near surface CII emissions, and a tangential TV which is used to obtain vertical and radial images of CII and CIII emissions near the target surfaces. In the benchmarking studies discussed here, MCI is used to calculate 2D densities distributions for each ionization state of carbon given a particular sputtering model. The CIII density is used to simulated λ = 464.7 nm CIII emissivities which are compared to line filtered CIII images from the DIII–D tangential TV. Similar studies have been carried out on JET with DIVIMP [18] and on Tore Suprawith BBQ [19].

3. Results and Discussion

Although the tangential TV is not absolutely calibrated it is useful for benchmarking the MCI carbon simulations. Shown in upper half of Fig. 1 is an experimentally measured CIII distribution for a typical radiative divertor shot just prior to detachment. The simulated CIII emission is shown in the lower half of Fig. 1. Here both physical and chemical sputtering, from the stand alone RG-R model, were used in MCI and the total steady state CIII inventory (*i.e.*, the CIII density spatially integrated over computational volume) is 4.12×10^{16} particles which results in an average CIII concentration of 0.01%. The total carbon inventory, contained in the MCI computational domain outside the 97% flux surface, is 6.11×10^{17} particles. This corresponds to an average carbon concentration of 0.182%. Neutral carbon is generated by the deuterium ion flux impinging on the target plates near inner and outer strike points in this single null diverted plasma. The carbon source distribution is illustrated in the lower frame of Fig. 2 with a target plate temperature of 373°K. The deuterium ion flux is shown in the upper frame of Fig. 2. The center frame shows the incident D^+ ion energy at the target plate as a function of the target plate segment number. Each segment in Fig. 2 represents the intersection of a cell boundary with the

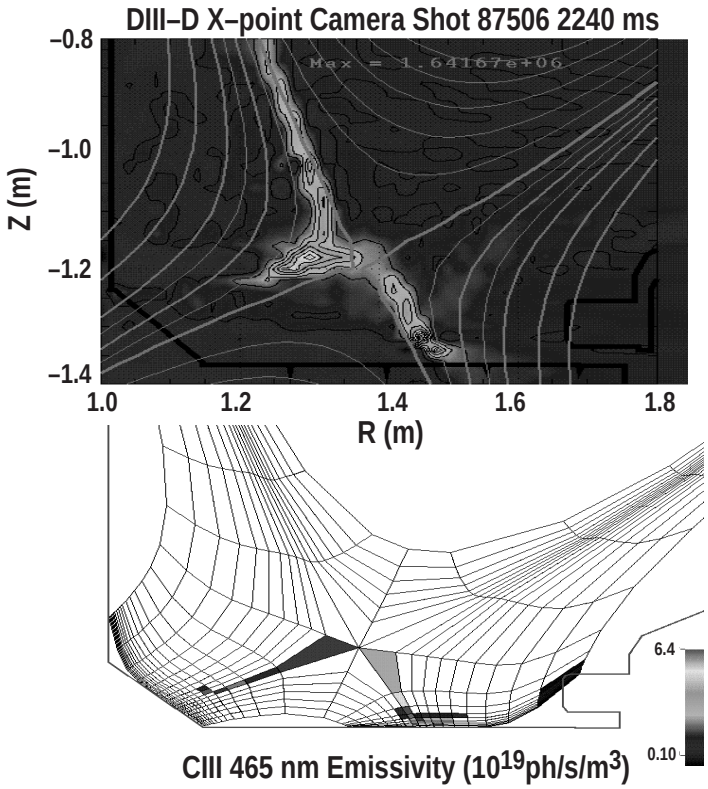

Fig. 1. Upper: experimental CIII emission, Lower: simulated CIII emission from MCI.

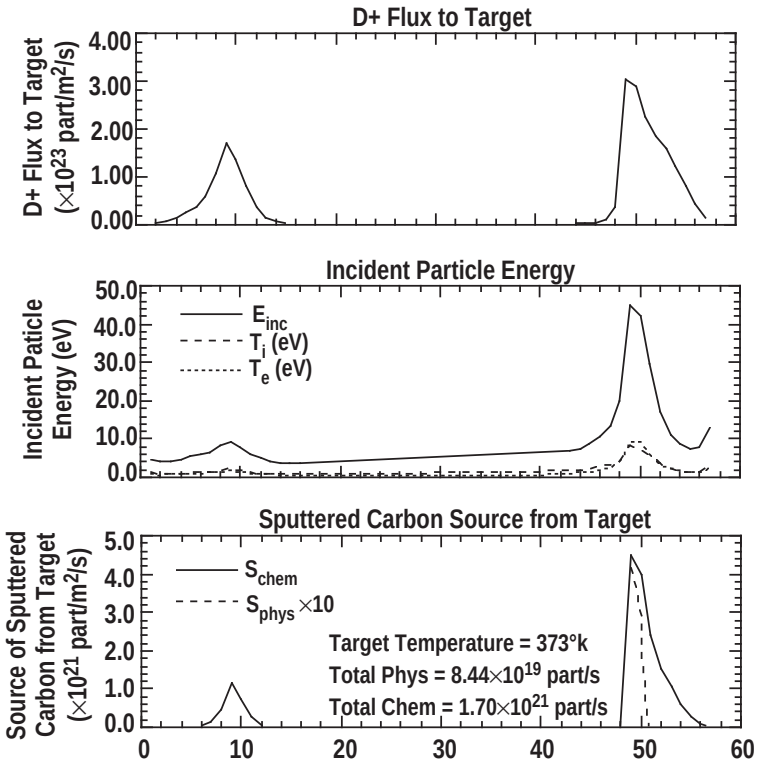

Fig. 2. Upper: Deuterium ion flux to the divertor targets, Center: energy of incident deuterium ions, Lower: simulated CIII emission from MCI.

divertor target plate starting from the inner most cell at the bottom of the grid, touching the inner wall, to the outer most cell which intersect the DIII–D baffle plate. Segments 10 and 49 represent the flux tubes bounded by the inner and outer strike points respectively.

Charge exchange neutrals are not accounted for in this simulation. These charge exchange neutrals produce additional carbon sources from the private flux region and the walls above the divertor region which may be significant for benchmarking. Work is in progress to include sputtering sources generated by the neutral deuterium flux.

Figure 2 illustrates the importance of using physics based sputtering models. This data was generated in MCI with a UEDGE background plasma which assumed a constant 10^{-3} sputtering yield. According to the RG-R model this *ad hoc* UEDGE sputtering assumption substantially underestimates the carbon source near the strike points (*i.e.*, the total UEDGE carbon source was 2.41×10^{20} particles/s whereas the RG-R models predict 1.78×10^{21} particles/s). In a cell just below the X–point, along the inner divertor leg, MCI indicates that the power radiated from the λ = 464.7 nm CIII line is 5.5×10^{-4} watts/m^3 with the UEDGE carbon source. The CIII radiation in this cell increases to 1.1 watts/m^3 when the RG-R sputtering source is used in MCI. The additional carbon from chemical sputtering appears to provide a mechanism for cooling the plasma near the X–point. This suggests that the comparison between MCI's CIII emissivities and the experimental data shown in Fig. 1

may be improved by the increased cooling rate implied from the MCI results. A clear demonstration of this hypothesis needs to be tested by regenerating the UEDGE background plasma with the MCI carbon distribution shown in Fig. 2. The regenerated background plasma could then be used in MCI to check for a convergence in the sputtering source and the CIII emissivity. An initial test of this iterative type of coupling between MCI and UEDGE is being planned.

4. Conclusions

Physical and chemical sputtering were compared in a pre-detached DIII–D divertor plasma. The carbon sputtering yield, due to chemical sputtering generated with the Roth and García-Rosales model, increased by about an order of magnitude near both the inner and outer strike points compared to physical sputtering with $Y=10^{-3}$. This increased the carbon inventory in the divertor and the power radiated by CIII near the X–point. The increase in CIII radiation is generally more consistent with experimental measurements but is as yet insufficient to validate the Roth and García-Rosales chemical sputtering model. A quantitative validation of the sputtering model is still needed.

Acknowledgements

The work discussed in this paper was sponsored by the U.S. Department of Energy under Contract Nos. DE-AC03-89ER51114 and W-7405-ENG-48.

References

[1] Rognlien, T.D., *et al.*, J. Nucl. Mater., **196-198** 347 (1992).
[2] Stangeby, P.C. and Elder, J.D., J. Nucl. Mater., **196-198** 258 (1992).
[3] Shimizu, K., *et al.*, J. Nucl. Mater., **220-222** 410 (1995).
[4] Evans, T.E., *et al.*, Proc. 10th Inter. Conf. Stellarators, IEA, 22-26 May 1995, Madrid, Spain.
[5] Stangeby, P.C., Contrib. Plasma Phys. **28** 507 (1988).
[6] Neuhauser, J., *et al.*, Nucl. Fusion **24** (1984) 39.
[7] Evans, T.E., *et al.*, Proc. Inter. Sherwood Fusion Theory Conf., 28 April 1997, Madison, WI.
[8] Stangeby, P.C., private communication, June 1997.
[9] Allen, S.L., *et al.*, Plasma Phys. Control. Fusion **37** A191 (1995).
[10] Fenstermacher, M.E., *et al.*, Rev. Sci. Instruments, **68** 974 (1997).
[11] Smith, D.L., J. Nucl. Mater., **75** 20 (1978).
[12] Smith, D.L., *et al.*, Proc. 9th Symp. on Eng. Prob. in Fusion Res., Chicago, 1981.
[13] Bohdansky, J., Nuclear Instr. Meth., **B2** 587 (1984).
[14] García-Rosales, C., Eckstein, W., Roth, J., J. Nucl. Mater., **218** 8 (1974).
[15] Roth, J. and García-Rosales, C., Nucl. Fusion **36** 1647 (1996).
[16] Thompson, M.W., Philos. Mag., **18** 377 (1968).
[17] Whyte, D.G., *et al.*, J. Nucl. Mater., **241-243** 660 (1997).
[18] Guo, H. Y., *et al.*, J. Nucl. Mater., **241-243** 385 (1997).
[19] Klepper, C.C., *et al.*, J. Nucl. Mater., 220–222 521 (1995).